For this purpose, we improved the on/off ratio of YLG by attaching another D-ring to fluorescein (YLGW, Fig. 1A). This modification reduced the potency and selectivity toward strigolactone receptors but improved signal resolution and stability. We used YLGW to visualize their response at 5-min intervals over 3 days (Fig. 3A, movie S1, and figs. S8 and S9). Within 20 min of YLGW application, fluorescence appeared at the root tip of the *Striga* embryo. The fluorescence diffused toward the cotyledon over 6 hours (the wake-up wave) and then disappeared (the pregermination pause). The loss of fluorescence may arise from leakage of the fluorescent dye produced, and it indicates a reduction of hydrolytic activity within the cell. Morphological signs of germination (root elongation) accompanied the second fluorescence wave from the root tip (the elongation tide). All germinating embryos (n = 13) followed these three stages, although with varying kinetics (fig. S9). The fluorescence dynamics depended on the hydrolysis of YLGW, because GR24 treatment alone did not generate fluorescence (movie S2 and fig. S9). The dynamics are also linked to germination, because the nonconditioned embryo showed nonspecific fluorescence over the entire embryo (movie S3 and fig. S9). Neither *Arabidopsis* (nonparasitic) nor *Phtheirospermum japonicum* (hemiparasitic), which are known to germinate independently of strigolactone, showed wavelike propagation of fluorescence (movies S4 and S5). These data suggest that the perception dynamics are related to strigolactone-dependent germination. Pulse-feeding experiments showed that *Striga* seeds require at least 6 hours of exposure to YLGW for efficient germination, corresponding to the completion of the wake-up wave (Fig. 3C). This observation indicates that the wake-up wave is necessary for efficient germination. RT-PCR analysis after GR24 treatment showed only mild induction in several *ShHTL*s, which suggests that transcriptional regulation of these genes is of limited importance in the perception dynamics (fig. S5).

The addition of ethylene results in the strigolactone-independent germination of *Striga* seeds, and this approach has been used to extirpate *Striga* seeds from farmers' fields (*1*). To further explore the relationship of strigolactone and ethylene with germination, we inhibited germination using either the ethylene biosynthesis inhibitor aminoethoxyvinylglycine (AVG) or the protein translation inhibitor cycloheximide (CHX) (*5*). Both compounds inhibited *Striga* germination induced by GR24 or YLGW in a dose-dependent manner (fig. S10). However, the response differed for YLGW-dependent fluorescence (Fig. 3, B, D, and E, and movies S6 to S8). AVG caused a loss of fluorescence intensity, whereas CHX delayed the arrival of the wake-up wave. Thus, protein translation is required to produce the factors that wake up the entire embryo by spreading competence to respond to strigolactones from the root tip.

Ethylene, the biosynthesis of which is induced by strigolactone signaling, enhances strigolactone perception and thus forms an amplification loop (*5*). This signal amplification may explain how *Striga* recognizes minute amounts of strigolactones in the soil.

We envisage that the identification of strigolactone receptors and the establishment of a small-molecule reporter system will accelerate research to combat *Striga*.

REFERENCES AND NOTES

1. G. Ejeta, in *Integrating New Technologies for Striga Control* (World Scientific Publishing, Toh Tuck Link, Singapore, 2007), pp. 3–16.
2. C. E. Cook, L. P. Whichard, B. Turner, M. E. Wall, G. H. Egley, *Science* **154**, 1189–1190 (1966).
3. B. Zwanenburg, A. S. Mwakaboko, *Bioorg. Med. Chem.* **19**, 7394–7400 (2011).
4. S. Toh *et al.*, *Plant Cell Physiol.* **53**, 107–117 (2012).
5. Y. Sugimoto *et al.*, *Physiol. Plant.* **119**, 137–145 (2003).
6. Y. Tsuchiya, P. McCourt, *Mol. BioSyst.* **8**, 464–469 (2012).
7. X. Xie, K. Yoneyama, K. Yoneyama, *Annu. Rev. Phytopathol.* **48**, 93–117 (2010).
8. K. Ueno *et al.*, *Phytochemistry* **108**, 122–128 (2014).
9. H. I. Kim *et al.*, *Phytochemistry* **103**, 85–88 (2014).
10. K. Yoneyama *et al.*, *New Phytol.* **206**, 983–989 (2015)
11. V. Gomez-Roldan *et al.*, *Nature* **455**, 189–194 (2008).
12. M. Umehara *et al.*, *Nature* **455**, 195–200 (2008).
13. K. Akiyama, K. Matsuzaki, H. Hayashi, *Nature* **435**, 824–827 (2005).
14. T. Arite *et al.*, *Plant Cell Physiol.* **50**, 1416–1424 (2009).
15. C. Hamiaux *et al.*, *Curr. Biol.* **22**, 2032–2036 (2012).
16. S. Toh, D. Holbrook-Smith, M. E. Stokes, Y. Tsuchiya, P. McCourt, *Chem. Biol.* **21**, 988–998 (2014).
17. A. Scaffidi *et al.*, *Plant Physiol.* **165**, 1221–1232 (2014).
18. Y. Seto *et al.*, *Proc. Natl. Acad. Sci. U.S.A.* **111**, 1640–1645 (2014).
19. K. Fukui *et al.*, *Bioorg. Med. Chem. Lett.* **21**, 4905–4908 (2011).
20. F. Chevalier *et al.*, *Plant Cell* **26**, 1134–1150 (2014).
21. C. Ruyter-Spira *et al.*, *Plant Physiol.* **155**, 721–734 (2011).
22. Y. Tsuchiya *et al.*, *Nat. Chem. Biol.* **6**, 741–749 (2010).
23. M. T. Waters *et al.*, *Development* **139**, 1285–1295 (2012).
24. F. Zhou *et al.*, *Nature* **504**, 406–410 (2013).
25. L. Jiang *et al.*, *Nature* **504**, 401–405 (2013).
26. Q. Liu *et al.*, *New Phytol.* **202**, 531–541 (2014).
27. J. Han, K. Burgess, *Chem. Rev.* **110**, 2709–2728 (2010).
28. J. W. J. F. Thuring, G. H. L. Nefkens, B. Zwanenburg, *Agric. Food Chem.* **45**, 1409–1414 (1997).
29. K. Sorefan *et al.*, *Genes Dev.* **17**, 1469–1474 (2003).
30. A. A. Awad *et al.*, *Plant Growth Regul.* **3**, 221–227 (2006).
31. S. Nakamura *et al.*, *Biosci. Biotechnol. Biochem.* **74**, 1315–1319 (2010).

ACKNOWLEDGMENTS

We thank A. Babikier for providing the *Striga* seeds; S. Yoshida and K. Shirasu for providing *Phtheirospermum* seeds; T. Nakagawa for the pGWB611 binary vector (*31*); M. Okumura for instructions on MEGA; E. Nambara for critical reading; H. Hirukawa and H. Tsuchiya for the artwork; and A. Miyazaki for proofreading the manuscript. This work was supported by the Advanced Low Carbon Technology Research and Development Program of the Japan Science and Technology Agency (643 to T.K.) and by a Grant in Aid for Scientific Research from the Ministry of Education, Culture, Sports, Science, and Technology (22119005 to T.K.). Y.T., S.T., D.H.-S., and P.M. were funded by the Natural Sciences and Engineering Research Council of Canada. A part of this work was supported by the Japan Advanced Plant Science Network. ITbM is supported by the World Premier International Research Center Initiative, Japan. Nagoya U. has filed for a patent (patent application no. 2015-132707) regarding the following topic: "Fluorescent probes and screening methods for the small-molecule regulators of germination in *Striga hermonthica*." Inventors: S. Hagihara, M. Yoshimura, Y. Tsuchiya, K. Itami, and T. Kinoshita. Nucleotide and amino acid sequences corresponding to *ShD14* and *ShHTL*s have been deposited in GenBank under accession numbers KR013120 to KR013131. YLG and YLGW are available from M. Yoshimura at Nagoya U. We declare no financial conflicts of interest in relation to this work. The supplemental materials contain additional data.

SUPPLEMENTARY MATERIALS

www.sciencemag.org/content/349/6250/864/suppl/DC1
Materials and Methods
Figs. S1 to S10
Table S1
Movies S1 to S8

20 April 2015; accepted 22 July 2015
10.1126/science.aab3831

RNA SPLICING

An alternative splicing event amplifies evolutionary differences between vertebrates

Serge Gueroussov,[1,2] Thomas Gonatopoulos-Pournatzis,[1] Manuel Irimia,[1,3] Bushra Raj,[1,2] Zhen-Yuan Lin,[4] Anne-Claude Gingras,[2,4] Benjamin J. Blencowe[1,2]*

Alternative splicing (AS) generates extensive transcriptomic and proteomic complexity. However, the functions of species- and lineage-specific splice variants are largely unknown. Here we show that mammalian-specific skipping of polypyrimidine tract–binding protein 1 (PTBP1) exon 9 alters the splicing regulatory activities of PTBP1 and affects the inclusion levels of numerous exons. During neurogenesis, skipping of exon 9 reduces PTBP1 repressive activity so as to facilitate activation of a brain-specific AS program. Engineered skipping of the orthologous exon in chicken cells induces a large number of mammalian-like AS changes in PTBP1 target exons. These results thus reveal that a single exon-skipping event in an RNA binding regulator directs numerous AS changes between species. Our results further suggest that these changes contributed to evolutionary differences in the formation of vertebrate nervous systems.

A major challenge in evolutionary biology is to determine which gene regulatory changes contributed to species-specific phenotypes (*1*–*3*). Comparative transcriptomic analyses revealed that vertebrate organ alternative splicing (AS) patterns diverged more rapidly than gene expression differences (*4*–*6*). These AS differences were largely attributed to changes in the use of conserved cis-regulatory elements (*4*, *5*). However, a small number of lineage- and species-

dependent AS changes were detected in nucleic acid–binding proteins, suggesting that splicing differences in trans-acting regulators also contributed to the extensive diversity found among vertebrates (*4*). One such change involves mammalian-specific skipping of an exon (exon 9 in humans, exon 8 in mice) in the polypyrimidine tract–binding protein 1 (PTBP1)/hnRNPI (*4*). PTBP1 controls cell- and tissue-dependent AS, as well as other steps in gene expression (*7*). Exon 9 encodes an intrinsically disordered and conserved linker between RNA recognition motif 2 (RRM2) and RRM3, two of the four RRMs in PTBP1 (Fig. 1A and fig. S1A).

To investigate the role of mammalian-specific exon 9 skipping, we performed RNA sequencing (RNA-seq) to profile AS in 293 cells engineered to express 3xFLAG-tagged PTBP1 transgenes with exon 9 included (PTBP1+Ex9) or deleted (PTBP1ΔEx9) (Fig. 1B and fig. S1B). In these cells, endogenous PTBP1 and PTBP2 [a paralog with partially redundant activity (*8*)] were depleted using small interfering RNAs (siRNAs). The percentage of transcripts with a sequence spliced in [percent spliced in (PSI)] was estimated for cassette exons [including 3 to 27 nucleotide microexons (*9*)], alternative 5′/3′ splice sites, and more complex AS events. The percentage of transcripts with an intron retained (PIR) was estimated for intron-retention events (*10*). AS events displaying an absolute ΔPSI or ΔPIR of ≥15% upon knockdown of PTBP1 and PTBP2, as well as a "rescue" of ≥50% of the levels observed in the control siRNA treatment, were analyzed further (supplementary materials and methods).

Approximately 1500 AS events showed differential regulation upon knockdown and rescue of PTBP1 (fig. S1C). Comparable proportions of most classes of AS events displayed increased and decreased PSI changes. In contrast, 67 and 92% of retained introns and microexons, respectively, showed increased inclusion levels upon PTBP1 knockdown ($P < 1 \times 10^{-8}$, hypergeometric test), consistent with recent findings (*11*). Comparison of the distributions of cassette exon ΔPSI values after induction of each PTBP1 isoform reveals that exon 9 inclusion results in significantly greater restoration of PSI values for both repressed (Fig. 1C, top panel) ($P < 1 \times 10^{-12}$, two-sided Mann-Whitney U test) and stimulated exons (Fig. 1C, bottom panel) ($P < 2.2 \times 10^{-16}$, two-sided Mann-Whitney U test). Reverse transcriptase polymerase chain reaction (RT-PCR) assays validated 23 of 23 analyzed RNA-seq predictions (Fig. 1, D and E, and fig. S2, A to C). Moreover, titration experiments confirmed that PTBP1+Ex9 and PTBP1ΔEx9 impart their distinct regulatory activities due to the presence and absence of exon 9 rather than differences in relative expression (fig. S3).

Recombinant PTBP1+Ex9 and PTBP1ΔEx9 proteins displayed similar binding affinities for a variety of RNA substrates in gel mobility shift assays (fig. S4). Moreover, in vivo cross-linking followed by immunoprecipitation (CLIP-seq) analysis revealed that these isoforms have near identical binding profiles surrounding PTBP1-regulated exons in vivo (fig. S5). Sequences overlapping RRM2 and exon 9 in PTBP1 define a minimal splicing repressor domain (*12*). Confirming this finding, deletion of this region markedly reduces PTBP1 splicing regulatory activity (fig. S6, A to C). However, the presence of exon 9 without RRM2 partially restores activity for a subset of analyzed target exons (fig. S6D). Collectively, these results indicate that exon 9 possesses splicing regulatory activity that is partially separable from the repressive activity conferred by RRM2 and

[1]Donnelly Centre, University of Toronto, Toronto, Ontario M5S 3E1, Canada. [2]Department of Molecular Genetics, University of Toronto, Toronto, Ontario M5S 1A8, Canada. [3]EMBL/CRG Systems Biology Research Unit, Centre for Genomic Regulation (CRG), Dr. Aiguader 88, 08003 Barcelona, Spain. [4]Lunenfeld-Tanenbaum Research Institute, Mount Sinai Hospital, 600 University Avenue, Toronto, Ontario M5G 1X5, Canada.
***Corresponding author. E-mail: b.blencowe@utoronto.ca**

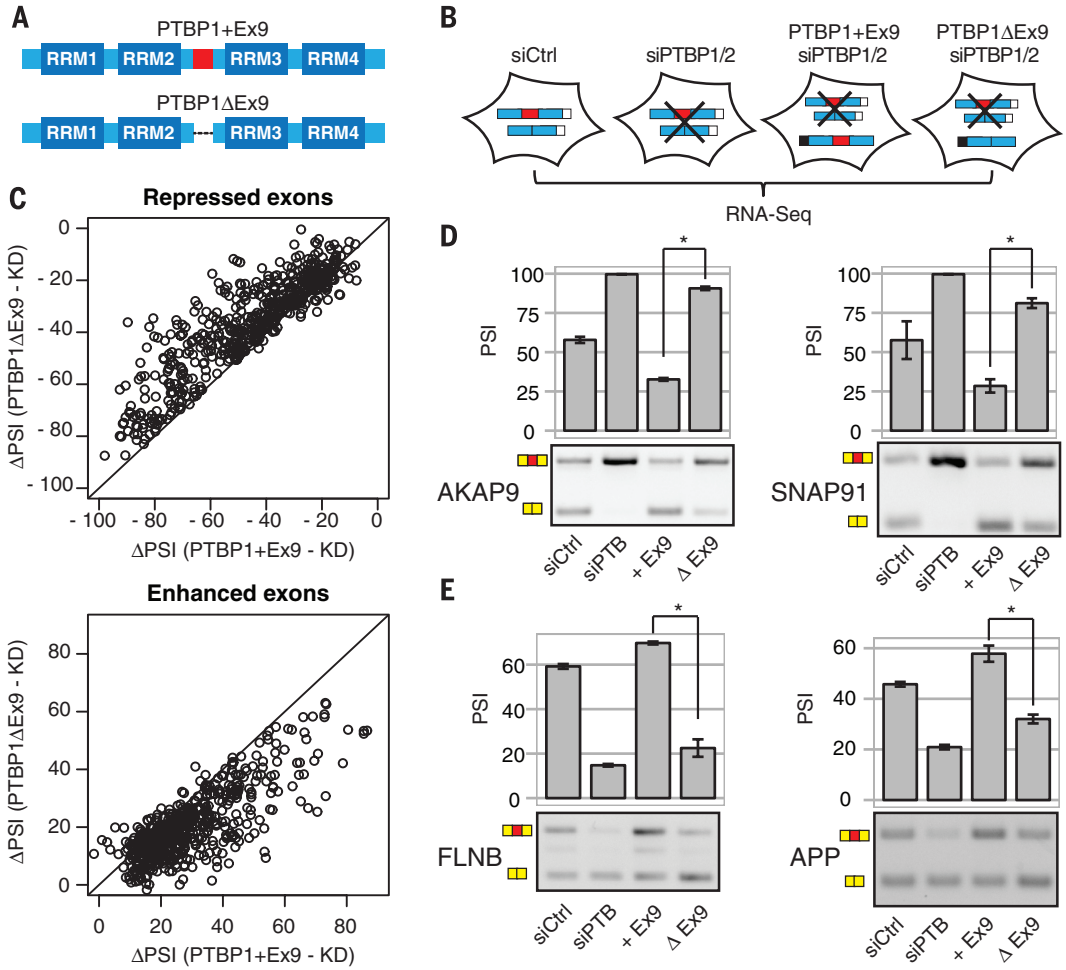

Fig. 1. A mammalian-specific AS event alters the global splicing regulatory activity of PTBP1. (**A**) Diagram showing the position of human PTBP1 exon 9. (**B**) Strategy for assessing the role of exon 9 in splicing regulation. Endogenous proteins were depleted with siRNAs. Knockdown was rescued with stably integrated, siRNA-resistant PTBP1+Ex9 or PTBP1ΔEx9. (**C**) Scatterplots showing changes in PSI relative to control for all cassette exons upon expression of PTBP1+Ex9 (*x* axis) or PTBP1ΔEx9 (*y* axis). (**D** and **E**) Representative RT-PCR validations of AS events, detected by RNA-seq, with inclusion (D) preferentially repressed by PTBP1+Ex9 or (E) preferentially enhanced by PTBP1+Ex9. Bar plots show mean PSIs from three independent RT-PCR experiments. Error bars denote SE. **P* < 0.05, two-tailed *t* test.

that skipping of exon 9 reduces the negative and positive regulatory activities of PTBP1 without substantially affecting RNA binding activity.

To investigate whether exon 9 inclusion influences splicing of PTBP1 target exons in other cell types, we investigated whether its PSI correlates significantly with PSI values of isoform-dependent and -independent target exons (fig. S7A) across 64 diverse human cell and tissue types (fig. S7B). As a control, we examined correlations between exon 9 PSI and PSI values of alternative exons that are not regulated by PTBP1. We observed a significantly higher correlation of exon 9 PSI with PSI of isoform-dependent target exons versus PSI of isoform-independent target exons or exons not regulated by PTBP1 (Fig. 2A, left panel) ($P < 1 \times 10^{-7}$, two-sided Mann-Whitney *U* test). These differences in correlation are not a consequence of isoform-dependent exons having a greater sensitivity to overall PTBP1 levels, because both isoform-dependent and -independent exons display a similar correlation with total PTBP1 mRNA levels (Fig. 2A, right panel) ($P = 0.40$, two-sided Mann-Whitney *U* test). Moreover, exon 9 PSI values do not correlate significantly with PTBP1 mRNA levels (fig. S7C) ($P = 0.66$, Pearson's product-moment correlation). Exons with inclusion levels that significantly correlate with the PSI of exon 9 ($P < 0.05$, Pearson's product-moment correlation) are enriched in genes functionally associated with cytoskeleton (e.g., *FLNB* and *MYO18A*) and nervous system development (e.g., *APP* and *APBB2*) (Fig. 2B, fig. S7D, and table S1). Thus, mammalian-specific skipping of exon 9 modulates the splicing levels of a large number of functionally coherent PTBP1 target exons across diverse cell and tissue types.

PTBP1 represses a network of neural-specific alternative exons in non-neural cells and tissues (*8*, *13*, *14*). Activation of this network is required for neuronal differentiation and depends on PTBP1 silencing by miR-124 (*8*, *13*, *14*). Many PTBP1-repressed exons are activated by the neuronal-specific Ser/Arg (SR)–related protein of 100 kD (nSR100/SRRM4) (*15*, *16*). Given that skipping of PTBP1 exon 9 reduces its repressive activity, we considered that this change might have evolved to further silence PTBP1 and render target exons permissive to activation by nSR100. To investigate this, we employed an in vitro model in which mouse embryonic stem (mES) cells are differentiated into cortical glutamatergic neurons (fig. S8, A and B). During differentiation, we observed the expected reduction in Ptbp1 and increase in nSR100 expression (*16*) (fig. S8C).

Concomitant with reduction of Ptbp1 mRNA levels, skipping of Ptbp1 exon 8 (orthologous to human exon 9) progressively increases during neuronal differentiation of two independent mES cell lines (CGR8 and R1) (Fig. 3, A and B, and fig. S8D). The transition from skipping to inclusion of exons that are negatively regulated by Ptbp1 and positively regulated by nSR100 begins between neuroepithelial stem cells and radial glia (*16*). This stage is associated with appreciable Ptbp1 mRNA expression but also corresponds to Ptbp1ΔEx8 supplanting Ptbp1+Ex8 (Fig. 3, A and B, and fig. S8D). These results suggest that preferential expression of Ptbp1ΔEx8 further derepresses the Ptbp1 and nSR100 coregulated neural AS network. Consistent with this proposal, Ptbp1 isoform-dependent exons, relative to Ptbp1 isoform-independent exons, display significantly higher inclusion early in the differentiation process (Fig. 3C and fig. S8E) ($P = 0.010$, two-sided Mann-Whitney *U* test) but exhibit significantly lower inclusion at later stages [i.e., between days 1 and 7 (T4 in fig. S8D); $P = 8.3 \times 10^{-5}$, two-sided Mann-Whitney *U* test]. To confirm whether Ptbp1ΔEx8 is a weaker repressor than Ptbp1+Ex8, we used in vitro splicing assays to compare the ability of each isoform to compete with nSR100. Splicing reporters containing neural-specific exons from the *PTBP2* and *Daam1* genes (*15*) were incubated with comparable amounts of recombinant nSR100, PTBP1+Ex9, and PTBP1ΔEx9 proteins (Fig. 3D and fig. S8, F and G). Relative to PTBP1+Ex9, PTBP1ΔEx9 has a reduced ability to outcompete nSR100 and promote skipping of each alternative exon.

To confirm whether Ptbp1 exon 8 skipping affects the kinetics of activation of neural exons in vivo, we used the clustered regularly interspaced short palindromic repeats (CRISPR)–Cas9 system to create mES cell lines that constitutively and uniquely express Ptbp1+Ex8 or Ptbp1ΔEx8 (Fig. 3E and fig. S9A). We then monitored Ptbp1

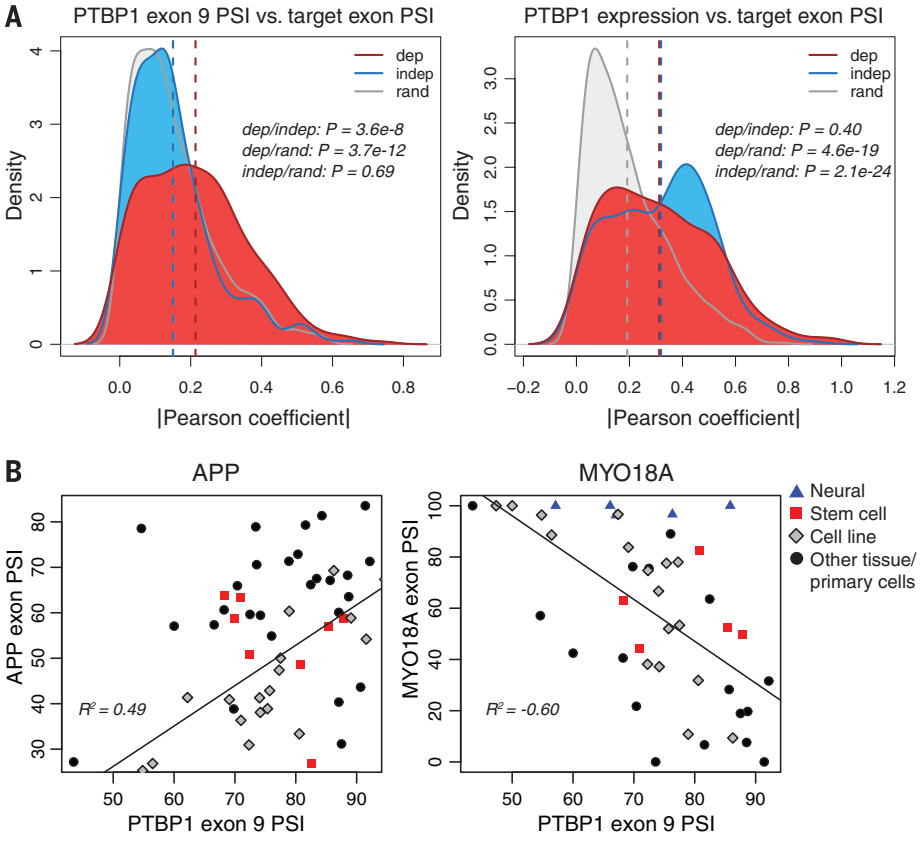

Fig. 2. PTBP1 exon 9 inclusion correlates with target exon inclusion across diverse human cells and tissues. (**A**) Analysis of Pearson correlation coefficients (PCCs) derived from RNA-seq comparisons of PTBP1 exon 9 PSI and PSIs of PTPB1 isoform-dependent target exons identified in Fig. 1. PCCs were computed from pairwise comparisons across 64 diverse human cell and tissue types (see supplementary materials). Plots show distributions of the absolute values of PCCs for different groups of target exons (dep, PTBP1-regulated and isoform-dependent; indep, PTBP1-regulated and isoform-independent; rand, not regulated by PTBP1). *P* values (two-sided Mann-Whitney *U* test) from comparing the indicated distributions are shown. (**B**) Scatter plots showing isoform-dependent PTBP1 targets whose PSI correlates significantly with PTBP1 exon 9 PSI across human cells and tissues (false discovery rate multiple testing correction; $P < 0.05$, Pearson's product-moment correlation).

target exon levels during differentiation of the lines into glutamatergic neurons. Expression of Ptbp1ΔEx8 resulted in earlier activation of target exons relative to that observed during differentiation of wild-type (WT) cells (Fig. 3F and fig. S9B). In contrast, constitutive expression of Ptbp1+Ex8 significantly delayed activation of the same targets (Fig. 3F and fig. S9B). Skipping of Ptbp1 exon 8 is therefore important for the activation of target exons during neuronal differentiation. Moreover, Ptbp1ΔEx8 expression led to earlier activation of key neural markers, whereas Ptbp1+Ex8 expression delayed their activation (Fig. 3G and fig. S10). These results demonstrate that a change in inclusion of a single alternative exon significantly affects the kinetics of regulatory transitions during mammalian neuronal differentiation.

Having established that skipping of exon 9 (or exon 8) reduces the regulatory activity of PTBP1 (or Ptbp1) in mammalian cells, we investigated

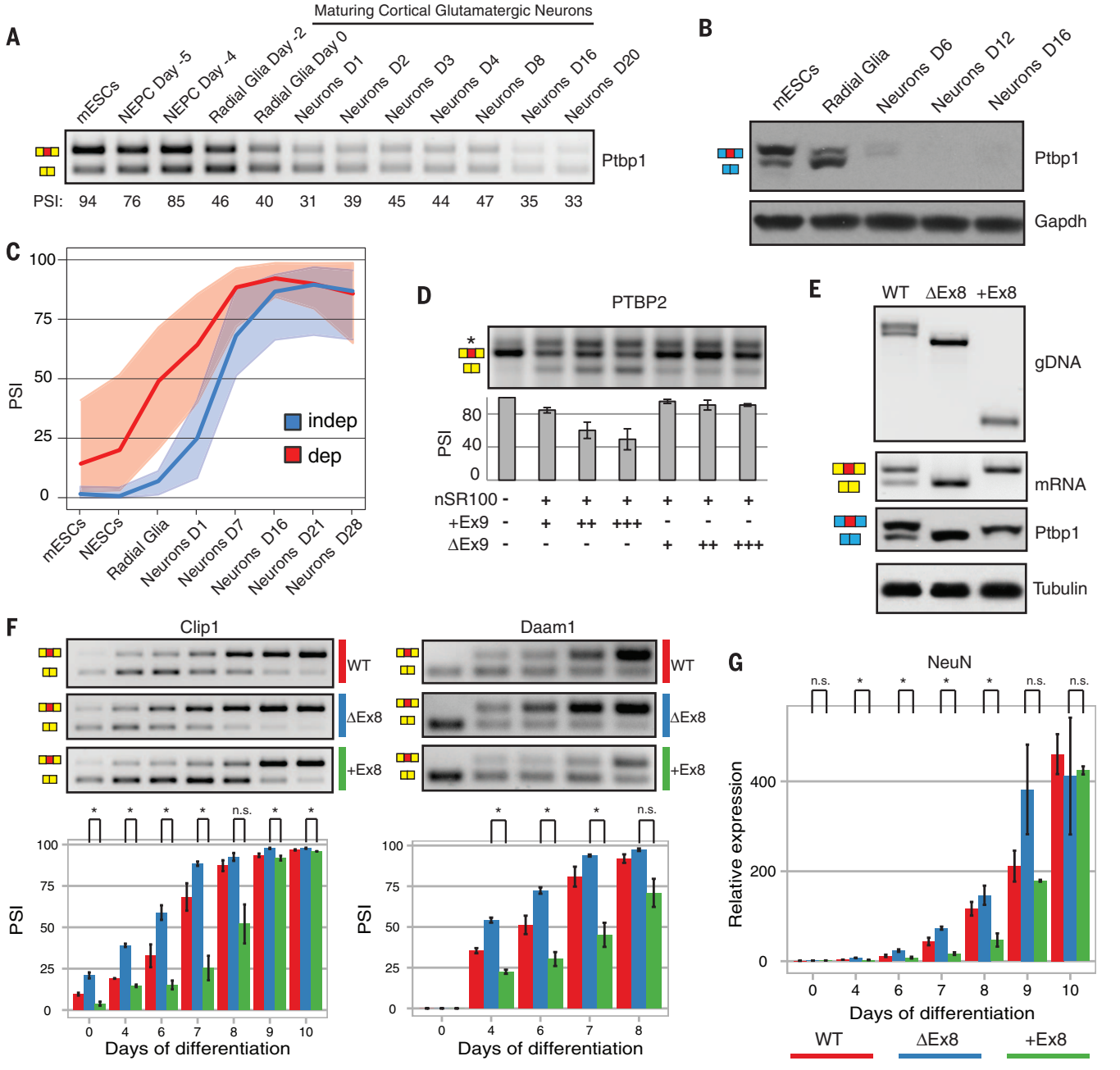

Fig. 3. Regulation and function of Ptbp1 isoforms during neuronal differentiation. (**A**) RT-PCR and (**B**) Western blot analysis of exon 8 inclusion during differentiation. mESCs, mouse embryonic stem cells; NEPC neuroepithelial stem cells; Gapdh, glyceraldehyde-3-phosphate dehydrogenase. (**C**) Plot of median Ptbp1 target exon PSIs during differentiation. Areas of lighter shading indicate the first and third quartiles. Red, mouse orthologs of human isoform-dependent events (dep); blue, isoform-independent events (indep). (**D**) In vitro splicing of PTBP2 exon 10 with varying combinations of purified nSR100, PTBP1+Ex9, and PTBP1ΔEx9. (**E**) Validation of CRISPR-Cas9–mediated deletion and knock-in of exon 8 at the level of genomic DNA (gDNA), RNA, and protein by PCR, RT-PCR, and Western blot, respectively. (**F**) Alternative splicing of Ptbp1-regulated exons was monitored by RT-PCR during differentiation in WT cells, cells with exon 8 deleted, or cells with exon 8 constitutively included. Quantification represents three independent differentiation experiments. Error bars indicate SE. *$P < 0.05$, two-tailed t test. n.s., not significant. (**G**) Expression of NeuN during differentiation was monitored by quantitative RT-PCR in the same lines. Quantification is as in (F).

whether introducing this mammalian-specific AS event in a nonmammalian context is sufficient to alter regulation of PTBP1 target exons. One or both copies of orthologous exon 8 were deleted in the chicken DT40 B cell line to generate cells that coexpress PTBP1+Ex8 and PTBP1ΔEx8 or that exclusively express PTBP1ΔEx8 (Fig. 4A). We performed RNA-seq analysis of the mutant and WT cell lines to assess the impact of exon deletion on the chicken transcriptome. Homozygous deletion of exon 8 resulted in splicing changes (PSI ≥ 15%) for 58 cassette exons, whereas heterozygous deletion resulted in intermediate changes in the same direction (Fig. 4B). Similar to the results in human cells, affected genes are enriched in gene ontology terms associated with the cytoskeleton (table S2). This set included exons in the *TPM1*, *MAGI3*, and *OSBPL9* genes whose human orthologs displayed isoform-dependent regulation in 293 cells. RT-PCR assays validated 24 of 31 (77%) analyzed events (Fig. 4C and fig. S11A). We further detected changes in exons of FLNB and PTBP2 (fig. S11B) that are isoform-dependent in 293 cells (Fig. 1E and fig. S2A) but had smaller predicted changes (PSI < 15%) in DT40 cells, possibly due to cell-type–specific contextual differences. In contrast, we did not detect significant changes in 12 of 12 exons not predicted to be affected by deletion of PTBP1 exon 8 (fig. S12). Affected exons probably comprise direct PTBP1 targets, because their flanking intronic sequences are significantly enriched in PTBP1 binding motifs (*17*), and the position of the enriched motifs is consistent with the expected direction of PTBP1-dependent regulation based on in vivo PTBP1 binding map data (fig. S5) (*18*, *19*) (Fig. 4D). Thus, expression of the PTBP1ΔEx8 isoform in chicken cells results in a weaker splicing regulator that leads to increased inclusion of PTBP1-repressed exons and reduced inclusion of PTBP1-stimulated exons. These results support the conclusion that an evolutionary change in PTBP1 exon 9 (or exon 8) inclusion is sufficient to alter the regulation of many exons, including those with important developmental functions.

Rapid evolutionary change in AS patterns has largely been driven by the gain and loss of

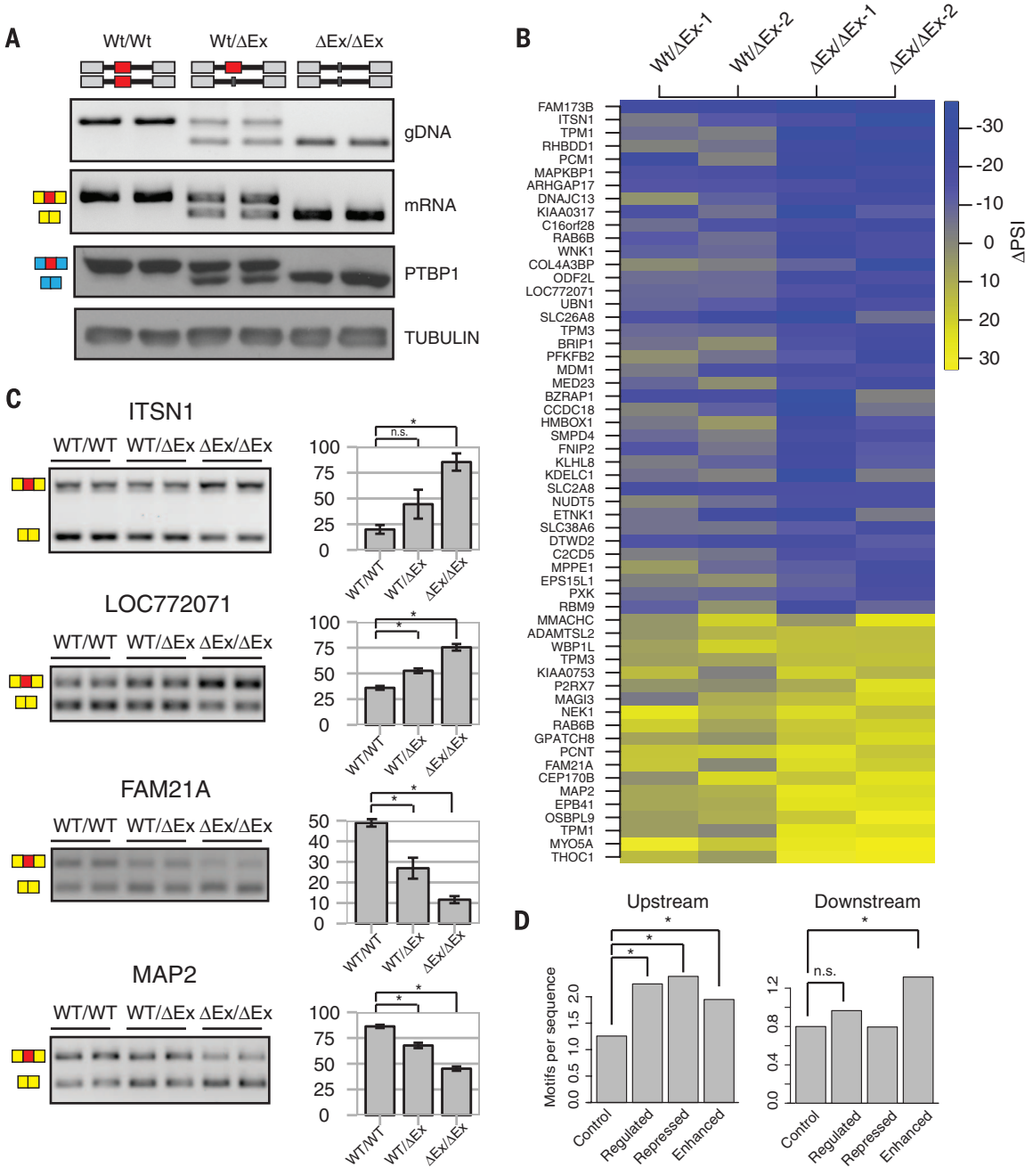

Fig. 4. Consequences of expressing a mammalian-like PTBP1 isoform in chicken cells. (**A**) Validation of heterozygous and homozygous deletions of PTBP1 exon 8 at the DNA, RNA, and protein levels by PCR, RT-PCR, and Western blot, respectively. (**B**) Heat map of average ΔPSI of exons affected by PTBP1 exon 8 deletion. Analyses were performed using two independent cell lines for each genotype. (**C**) Representative RT-PCR validations of AS events detected by RNA-seq. Bar plots show mean PSIs from six independent assays (three for each independent cell line). Error bars denote SE. *P < 0.05, two-tailed t test. n.s., not significant. (**D**) Number of PTBP1 motifs per 300 nucleotides of intronic sequence upstream (left) or downstream (right) of queried exons. *P < 0.05, exact binomial test.

cis-regulatory elements (*4*, *5*). It has been proposed that this change is partially a consequence of relaxed selection pressure acting on newly evolving splice isoforms, whereas the simultaneous expression of ancestral splice isoforms allows maintenance of core gene functions (*20*). However, the results of this study provide evidence that rapid change in AS can also be driven by splicing changes in trans-acting regulators. The mammalian-specific skipping of PTBP1 exon 9 (or exon 8), characterized here, simultaneously affects the levels of many additional AS events. Given that the affected target exons are concentrated in genes associated with cytoskeletal and neurobiological functions and that their regulatory kinetics are significantly affected by exon 8 inclusion levels during neuronal differentiation, this event may have evolved to modulate the timing of transitions in the production of neural progenitors and mature neurons so as to affect brain morphology and complexity. Thus, a single AS event has served to amplify the rate of evolutionary change in developmentally associated AS patterns.

REFERENCES AND NOTES

1. S. B. Carroll, *Cell* **134**, 25–36 (2008).
2. C. P. Ponting, *Nat. Rev. Genet.* **9**, 689–698 (2008).
3. A. Necsulea, H. Kaessmann, *Nat. Rev. Genet.* **15**, 734–748 (2014).
4. N. L. Barbosa-Morais *et al.*, *Science* **338**, 1587–1593 (2012).
5. J. Merkin, C. Russell, P. Chen, C. B. Burge, *Science* **338**, 1593–1599 (2012).
6. A. Reyes *et al.*, *Proc. Natl. Acad. Sci. U.S.A.* **110**, 15377–15382 (2013).
7. P. Kafasla *et al.*, *Biochem. Soc. Trans.* **40**, 815–820 (2012).
8. P. L. Boutz *et al.*, *Genes Dev.* **21**, 1636–1652 (2007).
9. M. Irimia *et al.*, *Cell* **159**, 1511–1523 (2014).
10. U. Braunschweig *et al.*, *Genome Res.* **24**, 1774–1786 (2014).
11. Y. I. Li, L. Sanchez-Pulido, W. Haerty, C. P. Ponting, *Genome Res.* **25**, 1–13 (2015).
12. F. Robinson, C. W. Smith, *J. Biol. Chem.* **281**, 800–806 (2006).
13. E. V. Makeyev, J. Zhang, M. A. Carrasco, T. Maniatis, *Mol. Cell* **27**, 435–448 (2007).
14. Y. Xue *et al.*, *Cell* **152**, 82–96 (2013).
15. J. A. Calarco *et al.*, *Cell* **138**, 898–910 (2009).
16. B. Raj *et al.*, *Mol. Cell* **56**, 90–103 (2014).
17. D. Ray *et al.*, *Nature* **499**, 172–177 (2013).
18. M. Llorian *et al.*, *Nat. Struct. Mol. Biol.* **17**, 1114–1123 (2010).
19. A. Han *et al.*, *PLOS Comput. Biol.* **10**, e1003442 (2014).
20. Y. Xing, C. Lee, *Nat. Rev. Genet.* **7**, 499–509 (2006).

ACKNOWLEDGMENTS

We thank A. Dziembowski for providing DT40-Cre1 cells, U. Braunschweig for assistance with CLIP-seq analyses, and N. Barbosa-Morais and T. Sterne-Weiler for advice on statistical testing. We also acknowledge D. Torti, D. Leung, and G. O'Hanlon in the Donnelly Sequencing Centre for generating RNA-seq data. S.G. is supported by a *Natural Sciences and Engineering Research Council* of Canada Alexander Graham Bell Studentship, T.G.-P. is supported by fellowships from European Molecular Biology Organization and Ontario Institute for Regenerative Medicine, and M.I. was supported by a Long-Term Fellowship from the Human Frontier Science Program. This research was supported by grants from the Canadian Institutes of Health Research to B.J.B. and A.-C.G. and by a Natural Sciences and Engineering Research Council of Canada John C. Polanyi Award to B.J.B. B.J.B. holds the Banbury Chair in Medical Research at the University of Toronto. Data presented in this manuscript are archived in the Gene Expression Omnibus under accession number GSE69656.

SUPPLEMENTARY MATERIALS

www.sciencemag.org/content/349/6250/868/suppl/DC1
Materials and Methods
Figs. S1 to S12
Tables S1 and S2
References (*21*–*25*)

4 February 2015; accepted 27 July 2015
10.1126/science.aaa8381

SIGNAL TRANSDUCTION

Membrane potential modulates plasma membrane phospholipid dynamics and K-Ras signaling

Yong Zhou,[1] Ching-On Wong,[1] Kwang-jin Cho,[1] Dharini van der Hoeven,[2] Hong Liang,[1] Dhananiay P. Thakur,[1] Jialie Luo,[1] Milos Babic,[3] Konrad E. Zinsmaier,[3] Michael X. Zhu,[1,4] Hongzhen Hu,[1,4] Kartik Venkatachalam,[1,4] John F. Hancock[1,4]*

Plasma membrane depolarization can trigger cell proliferation, but how membrane potential influences mitogenic signaling is uncertain. Here, we show that plasma membrane depolarization induces nanoscale reorganization of phosphatidylserine and phosphatidylinositol 4,5-bisphosphate but not other anionic phospholipids. K-Ras, which is targeted to the plasma membrane by electrostatic interactions with phosphatidylserine, in turn undergoes enhanced nanoclustering. Depolarization-induced changes in phosphatidylserine and K-Ras plasma membrane organization occur in fibroblasts, excitable neuroblastoma cells, and *Drosophila* neurons in vivo and robustly amplify K-Ras–dependent mitogen-activated protein kinase (MAPK) signaling. Conversely, plasma membrane repolarization disrupts K-Ras nanoclustering and inhibits MAPK signaling. By responding to voltage-induced changes in phosphatidylserine spatiotemporal dynamics, K-Ras nanoclusters set up the plasma membrane as a biological field-effect transistor, allowing membrane potential to control the gain in mitogenic signaling circuits.

Plasma membrane (PM) potential (V_m) has been linked to cell survival and proliferation (*1*, *2*). Dividing cells are more depolarized than quiescent cells, and oncogenically transformed cells are generally more depolarized than normal parental cells, indicating that V_m may be inversely coupled to pro-proliferative pathways (*2*). The mechanisms that might link V_m to cell proliferation are poorly characterized. Ras proteins are membrane-bound signaling proteins involved in cell differentiation, proliferation, and survival (*3*). The three ubiquitously expressed Ras isoforms—H-, N-, and K-Ras—assemble into spatially distinct nanoassemblies on the PM called nanoclusters (*4*). Nanocluster formation is essential for activation of mitogen-activated protein kinase (MAPK) signaling by Ras because activation of the protein kinase RAF on the PM is restricted to Ras.GTP (GTP, guanosine triphosphate) nanoclusters (*5*). Nanocluster assembly requires complex interactions between PM lipids and the Ras lipid anchors, C-terminal hypervariable regions, and G domains; with interactions between Ras basic residues and charged PM lipids being particularly relevant (*6*). The diffusion of lipids in model membranes and phase separation of multicomponent bilayers is responsive to electric fields (*7*, *8*). We therefore tested whether the lateral distribution of anionic lipids in the PM is responsive to V_m and the potential consequences on Ras spatial organization.

We manipulated the V_m of baby hamster kidney (BHK) cells, measured by whole-cell patch clamping, by changing extracellular K^+ concentration (Fig. 1A). Simultaneously we quantified the nanoscale distribution of various green fluorescent protein (GFP)–labeled lipid-binding probes on the inner PM by using electron microscopy (EM) and spatial mapping (*4*, *9*, *10*). The analyses show that nanoclustering of phosphatidylserine (PS) and phosphatidylinositol 4,5-bisphosphate (PIP_2) was enhanced on PM depolarization, whereas there was no detectable change in the lateral distribution of phosphatidic acid (PA) or phosphatidylinositol 3,4,5-trisphosphate (PIP_3) (Fig. 1, B and C, and fig. S1). The enhanced clustering of PS was fast, being 80% complete within 30 s (the shortest assay time allowed by the EM technique) (Fig. 1D). PIP_2 clustering increased at a slightly slower rate (Fig. 1D). On repolarization of the PM, by switching from 100 mM [K^+] back to 5mM [K^+], nanoclustering of PS and PIP_2 reverted to control values with near identical kinetics (Fig. 1E). The PS content of the PM was unaffected by changing V_m (fig. S2). Fluorescence recovery after photobleaching assays of lipid spatiotemporal dynamics showed that the mobile fraction of fluorescently labeled PS and PIP_2 decreased significantly upon PM depolarization (fig. S3), consistent with the EM data. The differential effect of V_m on anionic PM lipids is concordant with observations that charged lipids respond differently to applied electric fields (*7*, *8*, *11*).

[1]Department of Integrative Biology and Pharmacology, Medical School, University of Texas Health Science Center at Houston, Houston, TX 77030, USA. [2]Department of Diagnostic and Biomedical Sciences, Dental School, University of Texas Health Science Center at Houston, Houston, TX 77054, USA. [3]Department of Neuroscience, University of Arizona, Tucson, AZ 85721, USA. [4]Program in Cell and Regulatory Biology, University of Texas Graduate School of Biomedical Sciences, Houston, TX 77030, USA.
***Corresponding author. E-mail: john.f.hancock@uth.tmc.edu**

Editor's Summary

Regulation of splicing regulators

The messenger RNAs of most eukaryotic genes are formed by splicing together a series of exons and removing the intervening introns. The identity and order of the exons can vary between mRNAs for the same gene. The alternatively spliced products can generate an increased diversity of protein products. Gueroussov *et al.* show that the alternative splicing of a mammalian splicing regulatory factor affects, in turn, the alternative splicing of a wide range of target RNAs. This regulation mechanism controls a brain-specific alternative splicing program.

Science, this issue p. 868